PERGAMON

International Journal of Solids and Structures 36 (1999) 3277–3292

INTERNATIONAL JOURNAL OF SOLIDS and STRUCTURES

The stability of uniform-friction piles in homogeneous and non-homogeneous elastic foundations

Michael E. Heelis[a], Milija N. Pavlović[b,*], Roger P. West[a]

[a] *Department of Civil, Structural and Environmental Engineering, Trinity College, Dublin 2, Republic of Ireland*
[b] *Department of Civil and Environmental Engineering, Imperial College of Science, Technology and Medicine, London SW7 2BU, U.K.*

Received 10 February 1997; in revised form 23 September 1997

Abstract

The stability of piles that are supported vertically by a frictional force and laterally along their entire length by an elastic Winkler foundation is investigated for the case when the coefficient of subgrade reaction is either constant or varies linearly with depth and the friction is constant along the embedded length of the pile. A comparison between frictional and end-bearing models is made. Finally, a concise summary of the buckling loads for fully embedded friction piles is produced.

1. Introduction

Previous analytical treatments of the buckling of straight axially loaded piles completely embedded in elastic foundations have been based on the assumption that the foundations are homogeneous and the loading is concentrated at the extremities of the pile (Hetényi, 1946; Eisenberger and Yankelevsky, 1985; West et al., 1996). There are clearly many situations when these postulates are invalid (Terzaghi, 1955). However, it is generally accepted that the Winkler model does provide a reasonably accurate method for estimating the lateral response of piles (Pavlović and Tsikkos, 1982). The evaluation of the spring stiffness used in the Winkler model (also known as the modulus of subgrade reaction) varies with many parameters such as the breadth and stiffness of the pile and the intensity of the lateral load; guidance on its evaluation in the field may be found, for example, in CIRIA (1984) and West (1991).

This paper investigates the stability of a uniform-friction pile restrained by an elastic foundation of linearly varying modulus of subgrade reaction along its entire length using an exact closed-form

* Corresponding author. Fax: 0171 594 5989; E-mail: m.pavlovic@ic.ac.uk

0020–7683/99/$ - see front matter
PII: S0020–7683(98)00150–4

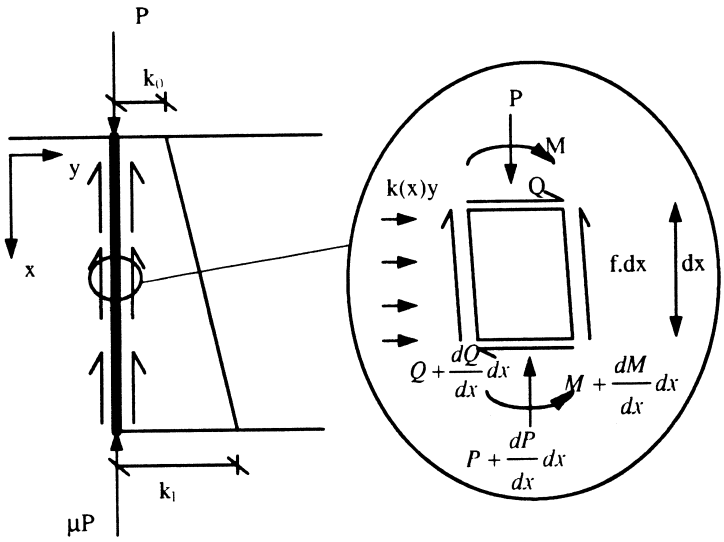

Fig. 1. A fully embedded pile in a linearly varying elastic foundation supported by a frictional force.

solution. In the formulation of the solution given in this paper any end conditions may be specified but the results discussed in detail are for fixed–fixed, pinned–pinned and free–free piles. The method outlined allows the investigation of both homogeneous and non-homogeneous subgrade-reaction cases, and also any proportion of the applied load to be supported by combinations of end-bearing or constant friction along the pile.

In this analysis the applied load remains vertical throughout and is resisted by shaft friction which is modelled as a vertical force distributed along the entire length of the pile shaft. The more complex case of a follower applied load is considered elsewhere using a discrete element approach (Smith, 1979). The springs of the Winkler foundation are perpendicular to the axis of the pile shaft and, hence, non-vertical piles can be analysed provided the modulus of subgrade reaction at right angles to the pile can be determined. This could lead to the applied load being eccentric to the axis of the pile. Although the solution to the latter problem is beyond the scope of this paper, it is outlined in principle at the end of the next section.

2. Method of analysis

Using a technique similar to that of Hetényi (1946) and taking an element dx of the pile in Fig. 1 it may be seen that, for moment equilibrium,

$$\frac{\mathrm{d}M}{\mathrm{d}x} - P(x)\frac{\mathrm{d}y}{\mathrm{d}y} - Q(x) = 0 \tag{1}$$

where $P(x)$ is the axial compressive force which is dependent on x, the distance along the pile, and $Q(x)$ is the shear force at a point x along the pile. These variables can be written as

$$M = -EI\frac{d^2y}{dx^2}, \quad P(x) = P_0 - fx \quad \text{and} \quad \frac{dQ}{dx} = k(x)y \tag{2–4}$$

where EI is the flexural rigidity of the pile member and is constant along its length in the present analysis, P_0 is the force in the pile at the top of the pile ($x = 0$), f is the friction per unit length of pile and $k(x)$ is the modulus of subgrade reaction. f is assumed to be constant and $k(x)$ is assumed to vary linearly with x, the distance below the top of the pile, so that

$$k(x) = k_0 + cx \tag{5}$$

where k_0 and c are constants for the foundation. k_l is defined as the maximum value of the stiffness parameter which exists at the base of the pile at $x = l$ (Fig. 1). The non-dimensional parameters μ and λ are introduced such that

$$\mu = \frac{P_l}{P_0}, \quad \lambda = \left(\frac{k_l l^4}{EI}\right)^{1/2} \tag{6}$$

where P_l is the load in the pile at the bottom of the pile ($x = l$). μ represents the proportion of the buckling load which is supported at the base of the pile and λ is the non-dimensional soil-stiffness parameter. In this way, piles completely supported by friction will have $\mu = 0$ and end-bearing piles with no friction will have $\mu = 1$. It follows that

$$f = \frac{P_0 - P_l}{l} = \frac{(1-\mu)}{l}P_0 \tag{7}$$

Differentiating (1) with respect to x and then substituting the variables from (2)–(5), the following is produced

$$EI\frac{d^4y}{dx^4} + (P_0 - fx)\frac{d^2y}{dx^2} - f\frac{dy}{dx} + (k_0 + cx)y = 0 \tag{8}$$

If the variable

$$\xi = \left(\frac{k_0 + cl}{EI}\right)^{1/4}(x - l) = \alpha(x - l) \tag{9}$$

is introduced, then

$$x = \frac{\xi}{\alpha} + l \tag{10}$$

It follows that

$$\frac{dy}{dx} = \alpha\frac{dy}{d\xi} \tag{11}$$

and, generally,

$$\frac{\mathrm{d}^n y}{\mathrm{d}x^n} = \alpha^n \frac{\mathrm{d}^n y}{\mathrm{d}\xi^n} \tag{12}$$

The governing equation with respect to ξ can now be formed as

$$\frac{\mathrm{d}^4 y}{\mathrm{d}\xi^4} + \left(\frac{P_0 - \frac{f\xi}{\alpha} - fl}{\alpha^2 EI} \right) \frac{\mathrm{d}^2 y}{\mathrm{d}\xi^2} - \frac{f}{\alpha^3 EI} \frac{\mathrm{d}y}{\mathrm{d}\xi} + \left(\frac{k_0 + \frac{c\xi}{\alpha} + cl}{\alpha^4 EI} \right) y = 0 \tag{13}$$

Now, let

$$\frac{P_0}{\alpha^2 EI} = \frac{P_0}{\sqrt{(k_l EI)}} = \beta \tag{14}$$

Hence

$$\frac{f}{EI\alpha^3} = \frac{(1-\mu)\beta}{\lambda^{0.5}} \tag{15}$$

and

$$\frac{fl}{\alpha^2 EI} = \frac{(1-\mu)P_0}{\alpha^2 EI} = (1-\mu)\beta \tag{16}$$

Also, let

$$\frac{k_0 + \frac{c\xi}{\alpha} + cl}{\alpha^4 EI} = \frac{k_l}{\alpha^4 EI} + \frac{c\xi}{\alpha^5 EI} = 1 + \gamma\xi \tag{17}$$

where,

$$\gamma = \frac{c}{\alpha k_l} \tag{18}$$

and let

$$\Gamma(\xi) = \mu\beta - \frac{(1-\mu)\beta\xi}{\lambda^{0.5}} \tag{19}$$

Hence, the dimensionless governing equation becomes

$$\frac{\mathrm{d}^4 y}{\mathrm{d}\xi^4} + \Gamma(\xi) \frac{\mathrm{d}^2 y}{\mathrm{d}\xi^2} - \frac{(1-\mu)\beta}{\lambda^{0.5}} \frac{\mathrm{d}y}{\mathrm{d}\xi} + (1+\gamma\xi) y = 0 \tag{20}$$

This is a fourth-order differential equation with variable coefficients. An exact solution is not available and, therefore, a power-series solution will be assumed. The solution is of the form

$$y = \sum_{n=0}^{\infty} a_n \xi^n \tag{21}$$

and by substituting it into (20), the following recurrence relationship between the coefficients a_n is produced

$$a_n = -\frac{\mu\beta(n-2)!a_{n-2}}{n!} + \frac{(1-\mu)(n-3)\beta(n-2)!a_{n-3}}{\lambda^{0.5}n!} - \frac{(n-4)!a_{n-4}}{n!} - \frac{\gamma(n-4)!a_{n-5}}{n!} \tag{22}$$

For any value of the parameter n, a_n may be written in terms of the first four terms in the series (a_0, a_1, a_2 and a_3). Therefore, a_n is a linear function of a_0, a_1, a_2 and a_3, and so the general solution to the differential equation is

$$y = \sum_{i=0}^{3} A_i Y_i \tag{23}$$

where

$$Y_i = \xi^i + \sum_{n=4}^{\infty} a_n \xi^n \tag{24}$$

and for $n < 4$, $a_n = 1$ if $n = i$ and $a_n = 0$ if $n \neq i$. A_0–A_3 represent the four constants of integration.

To obtain a buckling load of the pile and the corresponding mode shape, the boundary conditions at the ends of the member must be specified. If rotation is fully allowed, an expression for the bending moment at the pile end(s) must be obtained. When displacement in the y-direction is fully allowed, an expression for the shear force is required. The expressions for zero displacement, slope, bending moment and shear force with respect to the coordinate x are, respectively,

$$y = 0, \quad \frac{dy}{dx} = 0, \quad \frac{d^2y}{dx^2} = 0 \quad \text{and} \quad \left(\frac{d^3y}{dx^3} + \frac{P}{EI}\frac{dy}{dx}\right) = 0 \tag{25–28}$$

but, with respect to the coordinate ξ, they are,

$$y = 0, \quad \frac{dy}{d\xi} = 0, \quad \frac{d^2y}{d\xi^2} = 0 \quad \text{and} \quad \frac{d^3y}{d\xi^3} + \Gamma(\xi)\frac{dy}{d\xi} = 0 \tag{29–32}$$

The specification of the boundary conditions at the two ends of the pile yields four homogeneous equations, which can be expressed in a matrix equation,

$$[M]A = 0 \tag{33}$$

where M is formed using the following half-matrices to define all four possible instances of limiting boundary conditions (Fig. 2), with one half-matrix being evaluated at $x = 0$ and one at $x = l$;

$$[M_{\text{fixed}}] = \begin{bmatrix} Y_0(x) & Y_1(x) & Y_2(x) & Y_3(x) \\ Y_0'(x) & Y_1'(x) & Y_2'(x) & Y_3'(x) \end{bmatrix} \tag{34}$$

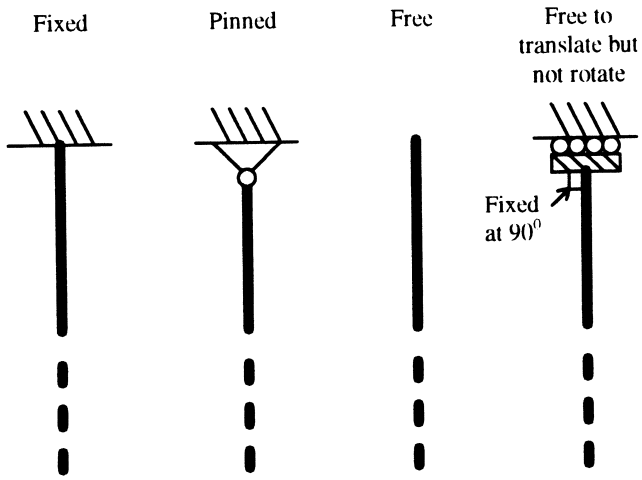

Fig. 2. The four cases of limiting boundary condition at the end of a member.

$$[M_{\text{pinned}}] = \begin{bmatrix} Y_0(x) & Y_1(x) & Y_2(x) & Y_3(x) \\ Y_0''(x) & Y_1''(x) & Y_2''(x) & Y_3''(x) \end{bmatrix} \tag{35}$$

$$[M_{\text{free}}] = \begin{bmatrix} Y_0''(x) & Y_1''(x) & Y_2''(x) & Y_3''(x) \\ Y_0''(x)+\Gamma(\xi)Y_0'(x) & Y_1''(x)+\Gamma(\xi)Y_1'(x) & Y_2''(x)+\Gamma(\xi)Y_2'(x) & Y_3''(x)+\Gamma(\xi)Y_3'(x) \end{bmatrix} \tag{36}$$

$$[M_{\text{no rotation}}] = \begin{bmatrix} Y_0'(x) & Y_1'(x) & Y_2'(x) & Y_3'(x) \\ Y_0''(x)+\Gamma(\xi)Y_0'(x) & Y_1''(x)+\Gamma(\xi)Y_1'(x) & Y_2''(x)+\Gamma(\xi)Y_2'(x) & Y_3''(x)+\Gamma(\xi)Y_3'(x) \end{bmatrix} \tag{37}$$

and

$$A = \begin{bmatrix} A_0 \\ A_1 \\ A_2 \\ A_3 \end{bmatrix} \tag{38}$$

The condition $|M| = 0$ gives the eigenvalues corresponding to the buckling load of the pile. A modified sign count algorithm is used to find the eigenvalues which are expressed in terms of ξ (West and Pavlović, 1993). Hence, the values of the constants of integration A_0–A_3 relative to each other are obtained for a particular eigenvalue and the buckling mode shape is calculated. (A note should be made regarding computations as $\lambda \to 0$: clearly, for $\lambda = 0$ there is a singularity because then $\alpha = 0$ which leads to $\lambda \to \infty$; however, the present algorithm works well for very small but finite λ (for example, $\lambda \approx 0.0001$).)

It is now convenient to introduce the following non-dimensional parameters, where the buckling force will be denoted as P_{crit}:

$$F = \frac{k_0}{k_l}, \quad \theta = \frac{P_{\text{crit}}}{P_{\text{E}}} \tag{39,40}$$

where P_{E} is the Euler buckling load of a simply supported beam with no elastic supports along its span and is given by $P_{\text{E}} = \pi^2 EI/l^2$. θ is the dimensionless buckling force as defined in Hetényi (1946).

It would be expected that, for the first buckling mode of an end-bearing simply supported pile, θ tends to one as the stiffness of the supporting medium tends to zero, while for a pile which is built-in at both supports, θ tends to four. These results are predicted by simple Euler theory. For the case of friction piles these limits no longer exist, but by using $\mu = 1$, an end-bearing pile can be modelled in order to verify the proposed method.

Note that, if the applied load on top of the pile was eccentric (or the pile was not vertical), then this could be analysed by modelling the eccentric loading as a moment and/or shear force at $x = 0$. This could be accommodated by the vector in eqn (33) no longer being a zero vector. While this would not alter the problem of the determination of the limiting eigenvalues (which is the principal object of the present work), there would be no proper bifurcation point but a steady increase in deflection which would rapidly tend to large values as the critical load was approached.

3. Results

To limit the number of graphs produced in this paper only the extreme cases of $\mu = 0$ and $\mu = 1$ will be examined initially though the method used can be applied to any value of μ. The extreme value of $\mu = 0$ gives an upper estimate for the evaluation of the buckling force because the axial force reduces along the pile length and, hence, the lower part of the pile is less likely to buckle. This means that the apparent length of the pile is reduced and the buckling load is increased. It should be noted that the case of $\mu = 1$ (the end-bearing case) is dealt with in depth in West et al. (1997). The two extreme cases of soil homogeneity ($F = 1$ and $F = 0$) in eqn (38) are, clearly, relevant to actual soil conditions as they approximate idealized unconsolidated clay and sand or consolidated clay conditions, respectively (Terzaghi, 1955). Varying F is also possible with the solution outlined above; however, discussion of the extreme cases means that differences in solutions are emphasized as much as possible and only upper and lower bounds of behaviour are provided. Hetényi (1946) demonstrated for end-bearing piles with uniform soil stiffness that, as the soil stiffness increases, there are predictable changes in the fundamental mode shape which can be characterized by the addition of a single half-wave (Fig. 3). Figure 3 also shows how the first and second buckling loads approach each other (before locally crossing over) for certain values of soil stiffness (for example at $\lambda \approx 30$); this is called a modal cluster. For symmetric boundary conditions (fixed–fixed, pinned–pinned and free–free) the theoretical buckling force can also be predicted exactly using a series of hyperbolic and trigonometrical expressions, as shown by Hetényi (1946). West et al. (1997) showed that, for end-bearing piles, when the soil stiffness is allowed to vary linearly with depth, these mode changes only occur at relatively weak soil stiffnesses, stabilizing to a mode shape with a constant number of half-waves as λ increases (say, approximately $\lambda > 150$—

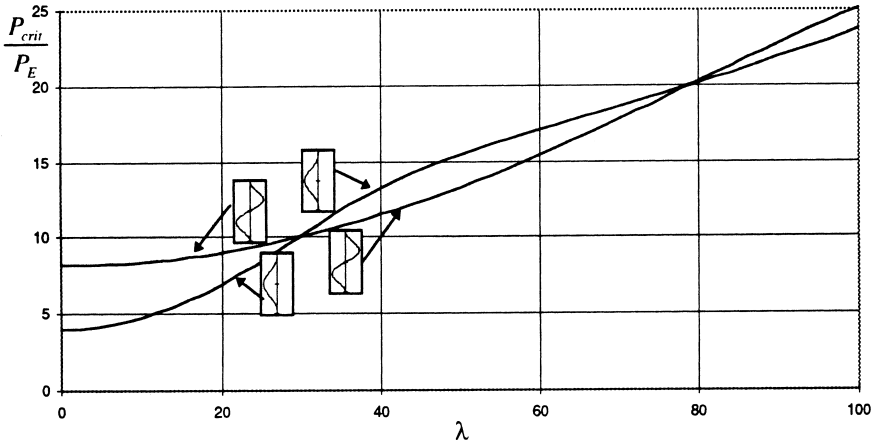

Fig. 3. First two buckling modes for a fixed–fixed end-bearing beam fully embedded in a homogeneous soil.

see Fig. 4). As expected, this mode shape is different to the Euler buckling mode shape that would exist if the soil was not present as discussed in West et al. (1997).

In verifying results by the use of a finite-element program using the method described by Lawther and Kabaila (1982) it was found that, when two modes are close together, the analysis would first converge on the second mode rather than the first mode; also, the mode shapes predicted would then be swapped and could be significantly different. This illustrates the necessity of adopting the present formal analytical approach. Additionally, it should be noted that, while the lowest mode

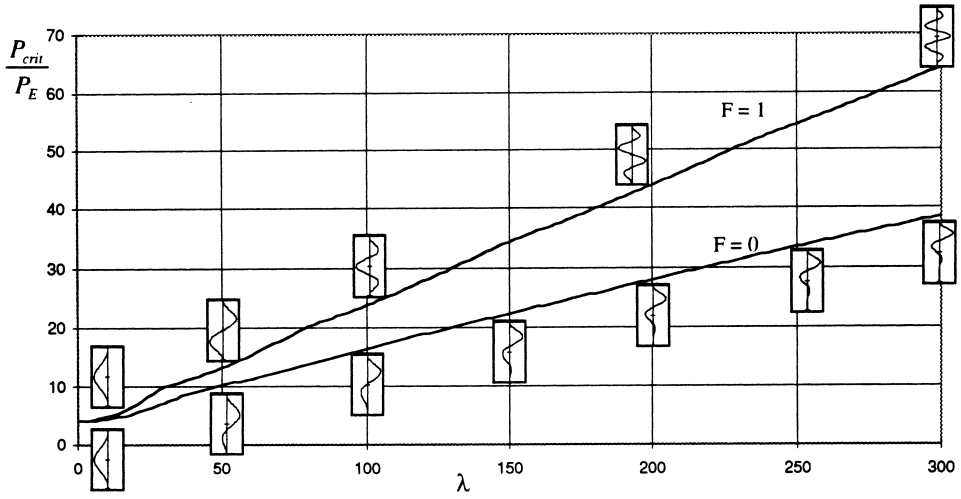

Fig. 4. First buckling mode for a fixed–fixed end-bearing beam fully embedded in a homogeneous ($F = 1$) and a non-homogeneous ($F = 0$) soil.

is the most significant, imperfections in the pile could mean that the second mode is produced. Also, attempts to strengthen a given pile by adding restraints with the aim of preventing particular modes from developing have to be carefully considered. Consequently, the inspection of higher modes in this work is used to establish whether there are any generic trends in their behaviour which will enable the prediction of trends in the lower modes which are hard to recognize if only the lowest modes are calculated.

In Fig. 5, the buckling loads are plotted for a beam fully embedded in a homogeneous soil with constant friction when the unembedded end-condition is fixed but the embedded end-condition is allowed to vary. The buckling loads do not depend on the embedded end-condition except at very low values of soil stiffness. It is thus possible to use any embedded end-condition. However, in the following discussion, symmetric boundary conditions will be used in order that parameters other than the boundary conditions can also be concentrated upon. The use of symmetric boundary conditions also allows a direct comparison with the results published for end-bearing piles in Hetényi (1946) and West et al. (1997).

Using the present analytical formulation, the buckling loads for a pile completely supported by friction and a pile completely supported by end-bearing are calculated and plotted in Fig. 6 for the fixed–fixed case. The friction case produces much higher buckling loads in all cases. The reason for this can be seen if the mode shapes in Fig. 7 are examined. In the friction case, for high λ, the buckling mode is concentrated in the top half of the pile, whereas for the end-bearing case the deflected shape extends along the whole pile. This non-symmetrical mode shape would be expected if the load distribution in the friction pile is considered. For instance, with $\mu = 0$, half-way down the pile the axial force would be equal to half the applied load at the top, while at the bottom of the pile the axial force is equal to zero; thus, if a crude average of the axial forces applied to the

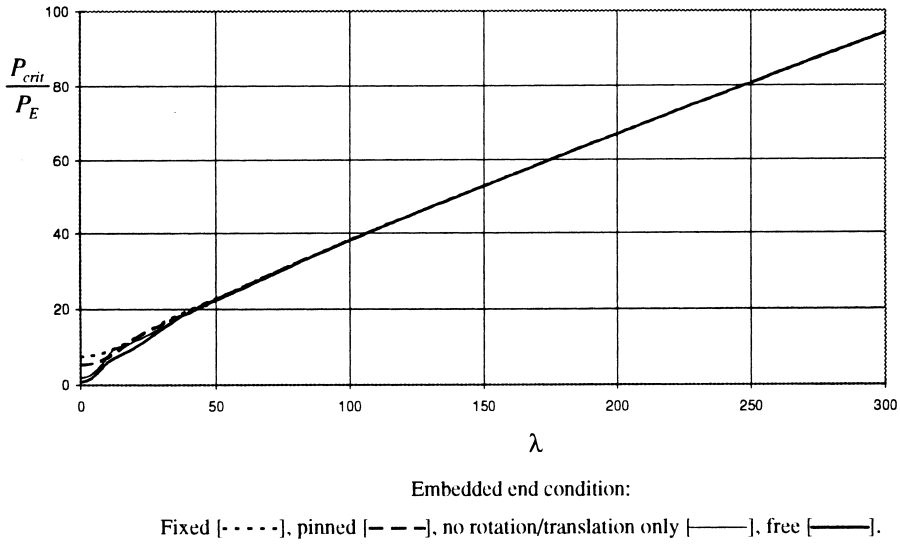

Fig. 5. First buckling mode for a fully embedded pure-friction beam with a fixed unembedded end and various conditions at the embedded end in a homogeneous soil with constant soil stiffness ($F = 1$) and constant shaft friction.

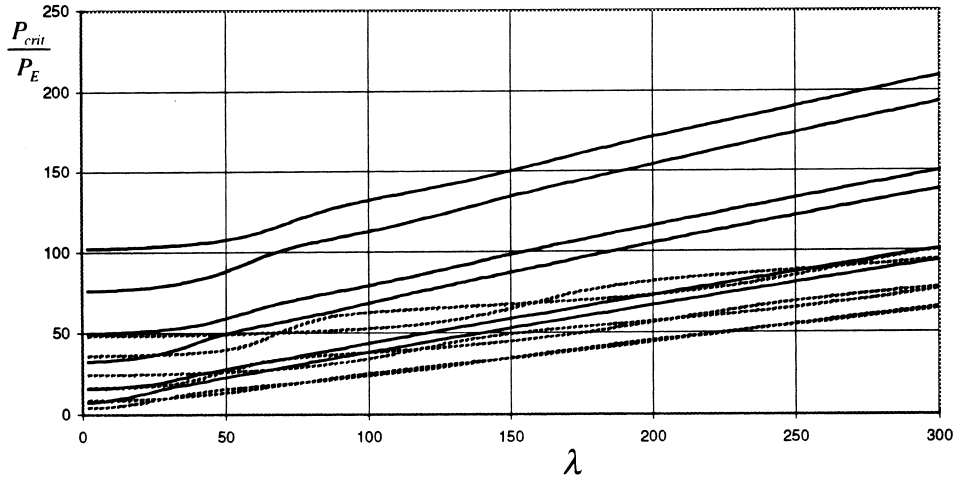

Fig. 6. First six buckling modes for a fixed–fixed pile with a constant soil stiffness supported entirely by either a constant frictional force or end-bearing (— $\mu = 0$, - - - $\mu = 1$).

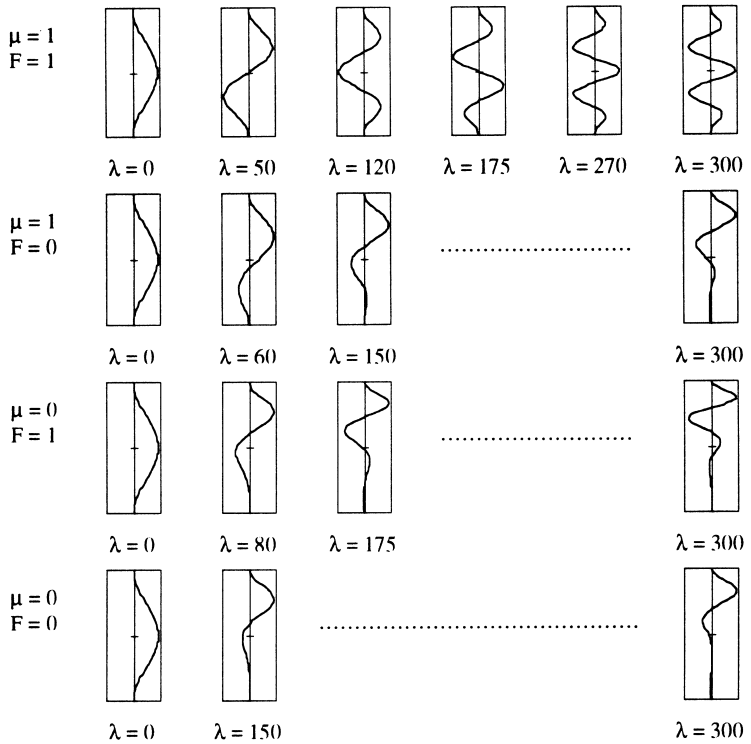

Fig. 7. Mode shapes for the first buckling mode as λ varies for the fixed–fixed case. (Some of the mode shapes are not shown (see dotted lines) as there is negligible variation in mode shape in this range.)

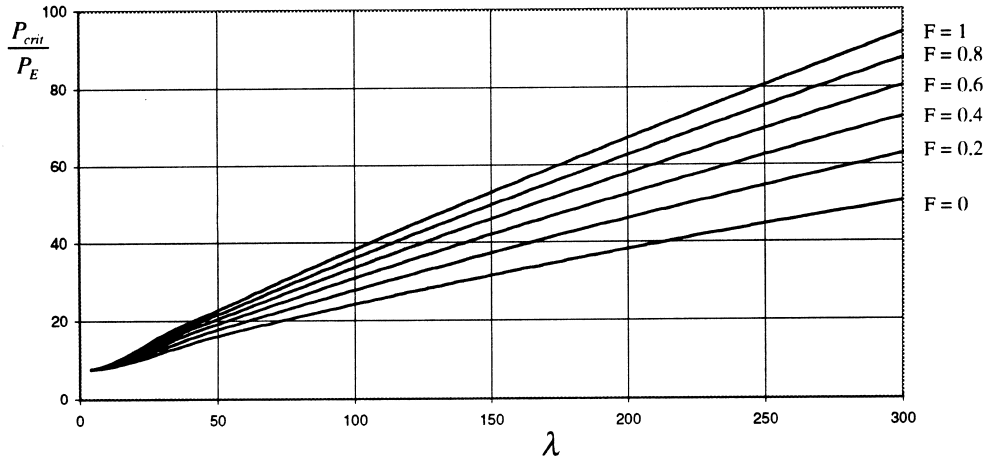

Fig. 8. First buckling mode for a fixed–fixed pile entirely supported by a constant frictional force along its embedded length as the soil homogeneity is varied.

top and bottom halves was taken, the average in the top half would be three quarters of the applied load, compared to only a quarter in the bottom half. Since in the homogeneous case the soil stiffness supporting both sections is the same, the top half would be more liable to buckle.

Consider again Fig. 6, where, despite the scale of the diagram, it is just possible to distinguish a series of modal clusters for the $\mu = 1$, end-bearing case. However, they are not present in the friction case except at the low end of the range of soil stiffnesses considered and, even here, the clusters are not as well defined as in the end-bearing case. Moreover, unlike the latter case, there is no cross-over of modes in the friction case. Hence, for all these reasons, from this point onward, the discussion will concentrate on the fundamental mode, which always provides a well-defined minimum, although it should be remembered that, especially for the range of soil stiffness $\lambda < 100$, the second mode may approach the first mode.

Figure 8 shows how the buckling loads vary when the soil stiffness changes between a constant and a linear variation with depth ($F = 1$ and $F = 0$, respectively) for a friction pile. As would be expected, the linear variation in soil stiffness produces piles with a lower buckling load compared to piles with a constant soil stiffness with depth. This is because the linear variation in soil stiffness supports the pile least where the amplitude of the mode shape is greatest, that is, near the soil surface. Figure 7, depicting the buckling modes for $F = 0$ and $F = 1$, shows how the effect of the non-homogeneity in the soil stiffness pushes the buckled shape upwards towards the more flexible soil at moderate to high values of λ. This is a similar effect to that of introducing the frictional support to the system. In Fig. 9 the results for linearly increasing soil stiffness for both cases (where the pile is supported by end-bearing and constant friction) are plotted. The results for the fundamental modes between $\mu = 0$ and $\mu = 1$ are not as separated compared to their counterparts in the constant soil-stiffness case (Fig. 6), because the non-homogeneity in the soil stiffness has already restricted the portion of the pile likely to buckle to where the decrease in the load in the pile is less pronounced, that is, at the top of the pile. This is reflected in Fig. 7 where the mode

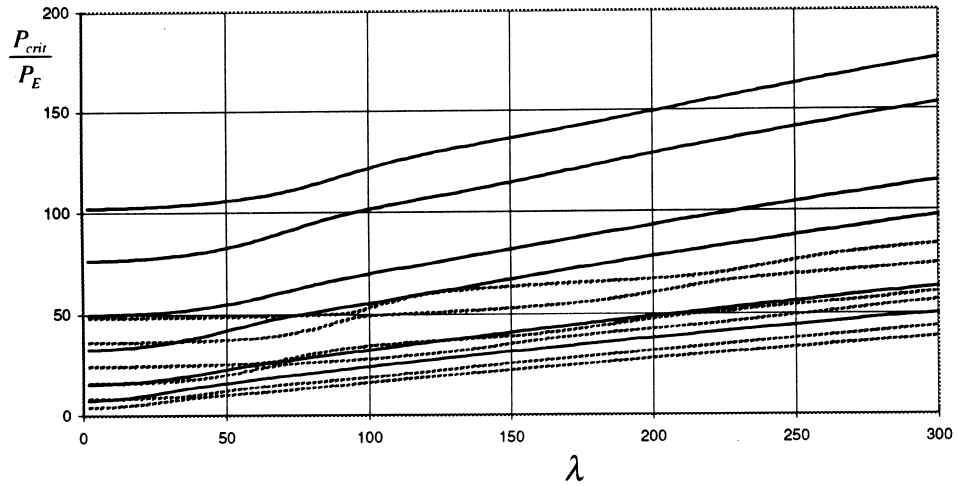

Fig. 9. First six buckling modes for a fixed–fixed pile with a linearly increasing soil stiffness supported entirely by either a constant frictional force or end-bearing (— $\mu = 0$, - - - $\mu = 1$).

shapes for $\mu = 0$ and $\mu = 1$ (for $F = 0$) are similar with maximum amplitudes of the mode shape at the top of the pile.

Figure 10 shows how the buckling load varies with soil stiffness for $F = 1$ for pinned–pinned end conditions as the load support mechanism varies from $\mu = 0$ to $\mu = 1$. Again, modal clusters tend not to appear in the friction case, as observed earlier for the fixed–fixed case. Note that the increase in the first mode between the end-bearing and the friction cases is only 25% compared to

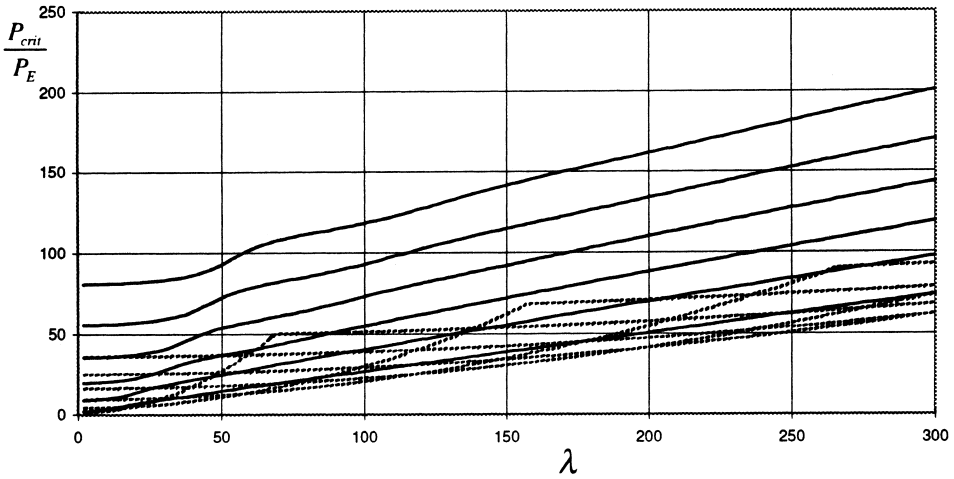

Fig. 10. First six buckling modes for a pinned–pinned pile with constant soil stiffness entirely supported by either a constant frictional force or end-bearing (— $\mu = 0$, - - - $\mu = 1$).

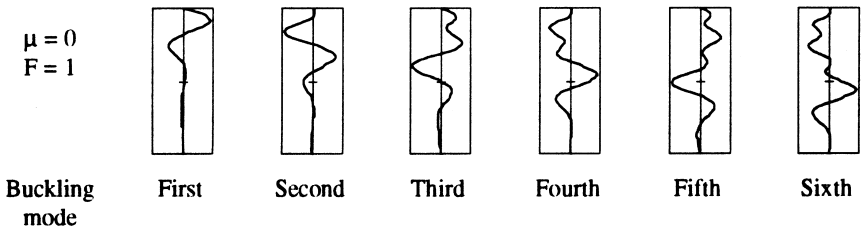

Fig. 11. First six mode shapes at $\lambda = 300$ for the pinned–pinned pile entirely supported by friction with a constant soil stiffness.

80% in the fixed–fixed case at $\lambda = 300$. The reason for this is that the large amplitudes of the mode shape can be closer to the top of the pile than in the fixed–fixed case. As mentioned previously this is the portion of the beam where the load in the pile changes least from the end-bearing to the friction case. Note that, for all except the lower stiffnesses, the modes from 1 to 6 are spaced evenly in the friction case whereas with the end-bearing results the mode shapes are paired (West et al., 1997). In Fig. 11 the first six modes at $\lambda = 300$ are plotted. The reason for the even spread of the buckling loads in Fig. 10 can be seen to be caused by the smooth progression of the wave with maximum amplitude and largest wavelength down the pile.

In Fig. 12 the results for the final symmetric problem with free–free ends are plotted. It should be noted that, for the end-bearing results (West et al., 1997), the first two modes are almost equal and cannot be readily distinguished using the scale on the diagram. The first mode of the friction case is almost identical to the results for $\mu = 1$, the difference at $\lambda = 300$ being less than 5%. The

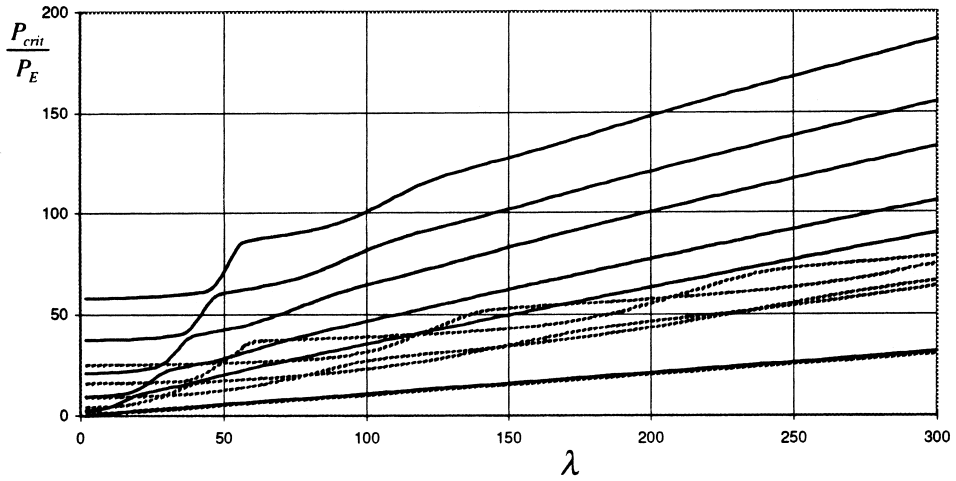

Fig. 12. First six buckling modes for a free–free pile with a constant soil stiffness entirely supported by a constant frictional force along its embedded length (— $\mu = 0$, - - - $\mu = 1$).

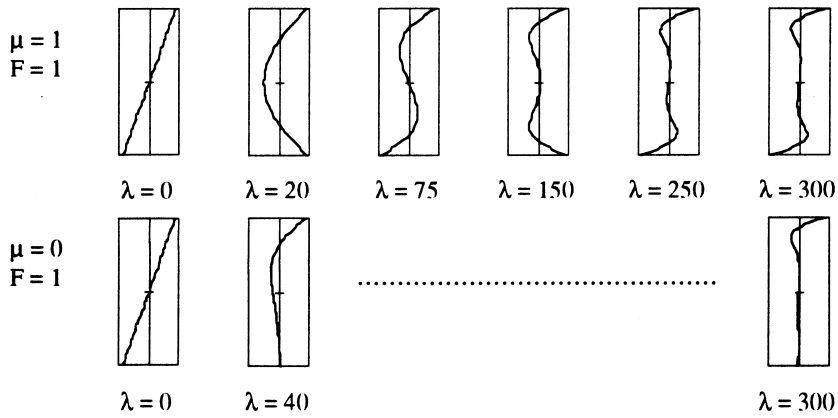

Fig. 13. Mode shapes for the first buckling mode as λ varies for the free–free pile entirely supported by friction with a constant soil stiffness. (See note for Fig. 6.)

second modes and above in the friction case are much higher. Figure 13 shows the first mode shapes for the end-bearing and friction cases as soil stiffness increases. Observe that for the fundamental mode in the friction case at low (but not zero) soil stiffness, there is a characteristic mode shape which does not change significantly as the soil stiffness increases.

In Figs 14 and 15 it is possible to plot a concise summary of the results for friction piles with the various unembedded end-conditions (since, as pointed out earlier, the embedded end-condition

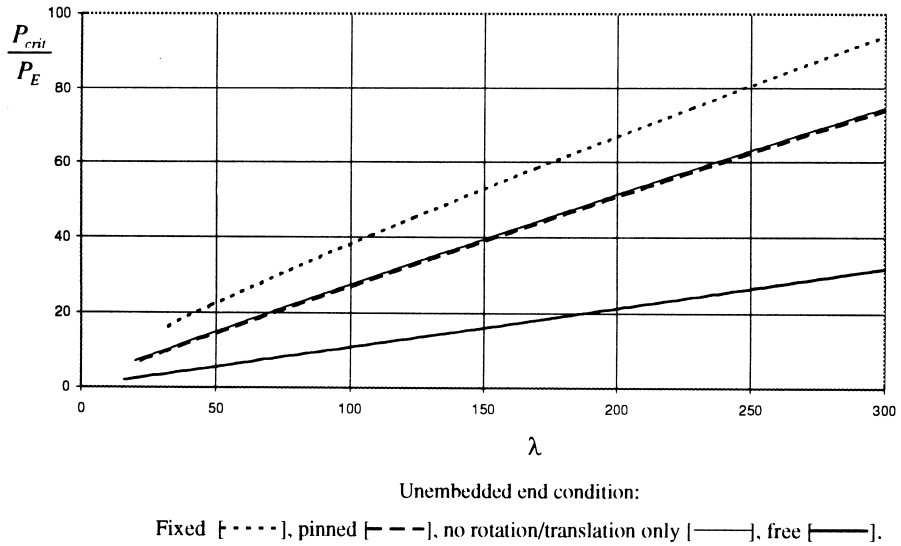

Fig. 14. First buckling mode for a fully embedded pure-friction beam with various conditions at the unembedded end in a homogeneous soil with constant soil stiffness ($F = 1$) and constant shaft friction.

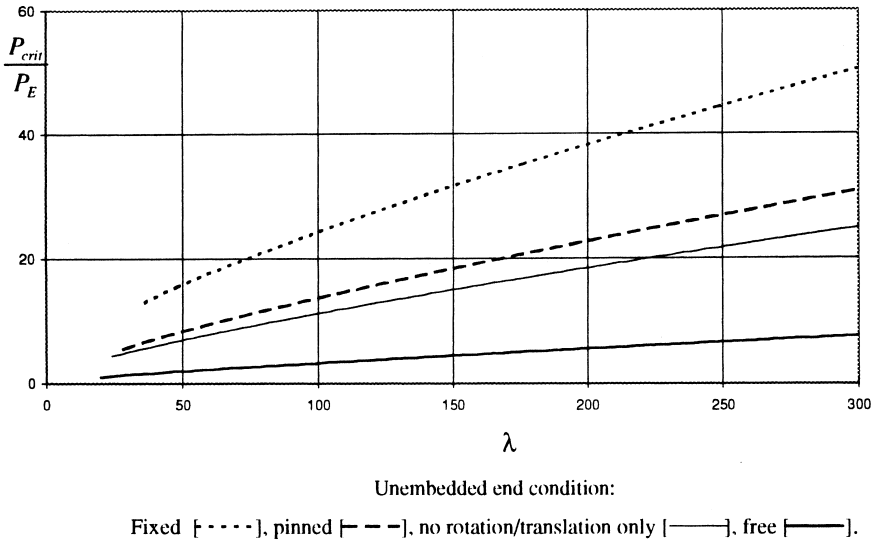

Fig. 15. First buckling mode for a fully embedded pure-friction beam with various conditions at the unembedded end in a non-homogeneous soil with triangular soil stiffness ($F = 0$) and constant shaft friction.

has practically no effect on the buckling load except at very low λ—see Fig. 5). The lines are the average of the buckling loads as the embedded end-condition is varied. At low soil stiffnesses the lines are not plotted if the maximum difference between the average and any one of the four embedded end-conditions exceeds 5%. The four limiting possibilities have been depicted in Fig. 2.

It is possible to extend the method herein to provide the solution to a layered soil model. Each layer may be homogeneous or non-homogeneous. Compatibility of deflection, slope, shear force and bending moment at the interface between each pair of layers can be combined with the boundary conditions at the top and the bottom of the pile, to provide sufficient equations to solve for the unknown coefficients. For a two-layered system this would mean that the final problem is expressed as an 8×8 matrix (see the partially embedded problem in Heelis, 1996). A three-layered problem would be defined by a 12×12 matrix, although, each row or column would only have a maximum of eight non-zero elements.

4. Conclusions

The dimensionless buckling loads and mode shapes for an Euler pile either completely supported by a constant frictional force along its entire length or purely end-bearing, and resting in a Winkler foundation have been presented. The soil-stiffness parameter of the Winkler foundation can either be constant with depth or vary linearly with depth, with either a zero or non-zero soil stiffness at the top of the pile. They were produced using an exact analytical solution to the governing differential equation and a powerful eigenvalue-solving algorithm on a standard computer.

The mode shapes for the previously studied problem of end-bearing piles with constant soil stiffness are significantly different to their counterparts for friction piles. The effect of either friction

or non-homogeneity of soil leads to the mode shape being concentrated in the upper portion of the pile and, hence, the mode shapes are not symmetrical or anti-symmetrical (as they were in the homogeneous end-bearing case). It may be concluded that the solution by Hetényi (1946) are of limited value in the prediction of mode shapes when either friction or non-homogeneity in the soil are liable to be present. Also, the effect of any rotational and/or displacement restraint at the pile foot is of minimal effect to the buckling mode shape for all but the lower range of values of the non-dimensional soil-stiffness parameter, much more so than when the soil is homogeneous and/or end-bearing prevails: nevertheless, for completeness, most plots cover all end-conditions for the embedded end, including the more realistic instance of a free (embedded) end.

With respect to the buckling loads that are predicted, there is no generic trend across all the different end conditions. Taking values at $\lambda = 300$, the increase in buckling load for the friction support compared to the end-bearing support are around 80, 25 and 5% for the fixed–fixed, pinned–pinned and free–free end conditions, respectively, for the first mode. This means that there is no simple guideline or equation which can be employed to predict the increase in buckling load produced by the addition of friction to the model and, hence, a series of non-dimensional graphs have presently been produced from which the buckling load of a friction pile in either an homogeneous or a non-homogeneous soil may be predicted.

Acknowledgement

The authors would like to express their thanks to the two reviewers for their careful reading of an earlier draft of the article and for making helpful suggestions for its improvement.

References

CIRIA, 1984. Design of laterally loaded piles. CIRIA Report 103, London.

Eisenberger, M., Yankelesvsky, D.Z., 1985. Exact stiffness matrix for beams on elastic foundation. Computers and Struct. 21, 1355–1359.

Heelis, M.E., 1996. The stability of fully and partially embedded beam-columns in elastic Winkler foundations. Ph.D. thesis, Trinity College, Dublin.

Hetényi, M., 1946. Beams on Elastic Foundation. University of Michigan Press, Ann Arbor.

Lawther, R., Kabaila, A.P., 1982. Modification of the power method for determination of eigenvalues. Proc. 4th Int. Conf. on Finite Elements in Australia. University of Melbourne.

Pavlović, M.P., Tsikkos, S., 1982. Beams on quasi-Winkler foundation. Engng Struct. 4, 113–118.

Smith, I.M., 1979. Discrete element analysis of pile instability. Int. J. Num. and Anal. Methods in Geomech. 3, 205–211.

Terzaghi, K., 1955. Evaluation of coefficients of subgrade reaction. Geotechnique 5, 297–326.

West, R.P., 1991. Modal clustering in the vibration of beams partially embedded in a Winkler foundation. Ph.D. thesis, Trinity College, Dublin.

West, R.P., Pavlović, M.P., 1993. A fast iterative algorithm for eigenvalue determination. In: Topping, B.H.V. (Ed.), Developments in Computational Eng. Mech., Civil-Comp. Press, pp. 229–236. (Reprinted in: 1997 Computers and Struct. 63, 749–758.)

West, R.P., Heelis, M.E., Pavlović, M.N., Wylie, G.B., 1997. The stability of end-bearing piles in a non-homogeneous elastic foundation. Int. J. Num. and Anal. Meth. in Geomech. 21, 845–861.